7.3 Beam shaping

M. Scholl

7.3.1 Introduction

Beam shaping [97Aag, 99Sin, 00Dic] as a technical term is not clearly defined. In most relevant cases the task of beam shaping is as follows: generate by some optical system a spatial Power Density Distribution (PDD) with certain desired features from a given input beam – at least to some approximation. The requirements on the desired PDD result from the applications the beam is used for, e.g. adapting the intensity distributions for laser materials processing or splitting beams for multiplexing in optical communication. An important example is the generation of highly homogenous rectangular beam profiles for illumination of masks in lithography, for annealing applications or for digital light processors in video projection devices. In all these cases the transformation of the PDDs must be done with minimum loss of beam power to ensure the efficiency of the subsequent applications. This restriction usually rules out mask projection techniques which typically apply absorbing masks. Consequently, the characteristic feature of beam shaping is the use of pure phase masks to generate the desired output beam.[1]

Sometimes the term beam shaping is used for the compensation of the ellipticity of astigmatic beams, too [99Sin, 00Dic]. Mostly this is done with ABCD-transformations realized with the help of quadratic phase elements, typically cylinder lenses. In a sense ABCD-transformations do not affect the internal structure of the PDD. In the spirit of the examples quoted above the term beam shaping applies only for non-quadratic phase transformations of the PDD which cannot be performed by ABCD-systems. In this contribution beam shaping will be used in this restricted sense in connection with non-quadratic phase elements only.

Furthermore, in situations where the typical time constant of the subsequent process allows fast sequential illumination of different parts of the PDD beam scanning may often be the simplest and most economical way to shape the required PDD. This should be checked first. Beam scanning, however, is a non-stationary technique which will not be considered here.

The most common stationary beam-shaping techniques which are used to generate a shaped PDD are beam transformation [96Hen, 97Aag, 00Dic, 03Ber], which shows the basic technique, beam integration [88Dic, 96Hen, 98Unn], combined beam integration with beamlet shaping [96Hen, 99Pah, 03Ber] and beam splitting [97Aag, 99Sin].

A typical arrangement for all these methods is shown in Fig. 7.3.1, which shows the basic idea of beam shaping: At the input plane (x_0, y_0) located at $z = 0$ the wavefront of the incoming beam is deformed by a phase element. The phase element forms a new wavefront in the plane (x', y') at $z' = 0 + \varepsilon$ in such a way that the desired PDD $I_1(x_1, y_1)$ builds up in the plane (x_1, y_1) at position z_1 behind some paraxial optical system. The phase element can be realized either by a mirror or by transmissive optics with an appropriate surface structure. The differences in the various beam-shaping techniques can be traced back to the properties of the structure function d of the phase element.

[1] However, using phase elements only it is difficult to generate abrupt intensity changes and highly structured profiles. For applications where high resolution is of prominent importance like in lithography lossy mask projection techniques are an indispensable tool.

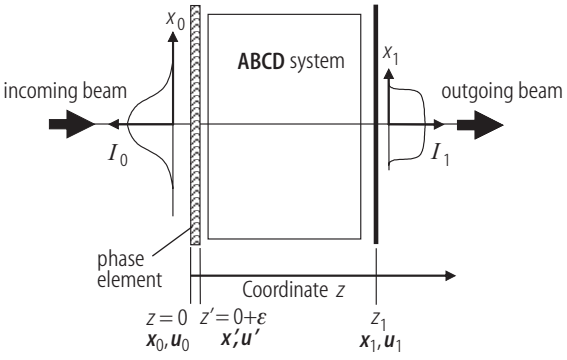

Fig. 7.3.1. Typical arrangement used in beam-shaping applications. The different shapes of the input and output PDDs $I_0(x_0, y_0)$, $I_1(x_1, y_1)$ are sketched.

For beam transformation a one-to-one mapping between points of the input and the output plane is assumed. A deterministic and invertible redistribution of the power in the PDD is inferred by the structure function. In beam transformation it is possible to perform an even more complete beam shaping by adjusting also the phase of the output beam with an appropriate second phase element. However, the input beam has to be known very precisely to determine the structure function. The technique is sensitive to deviations from the specified situation and to misalignment.

For the shaping of homogenous tophat profiles these disadvantages can be avoided by beam integration. The basic idea of beam integration by multifaceted mirrors or lenses is cutting the beam profile in segments called beamlets and superposing them in the output plane. The superposition acts as averaging of the beamlet profiles and a homogenous profile results. Due to the superposition of the beamlets a point in the output plane now has several preimages. In contrast to beam transformation there is no one-to-one correspondence between points in the input and output plane. Additional phase corrections in the output plane are not possible. Because of the segmentation the structure function d is periodic up to quadratic contributions.

Output PDDs different from tophats may be obtained by combining beam integration and beam transformation. This technique supposes that for each facet the input beamlet may approximately be treated as a plane-wave segment. The facet surfaces are structured appropriately so that the output profile is formed from this plane-wave segment by the facet. The superposition again averages possible differences and deviations in the output profiles.

Beam integration with beamlet shaping is much less sensible and may be applied if knowledge of the input beam is poor.

As coherence influences the result of beam shaping the design of the optics must take into account the coherence parameters [96Hen, 98Unn]. For beam integrators this crudely means that the facet width approximately should be of the order of the transverse coherence length of the beam.

Beam splitting differs from the previously quoted techniques in the structure of the output PDD. Usually an array of peaks with disjoint support has to be shaped. For a coherent beam this can be done with periodic structure functions. In this respect the situation is similar as in beam integration.

Manufacturing of beam-shaping elements requires methods to realize free form surfaces for mirrors or transmissive elements. Fast tool servo diamond turning machines are an appropriate tool for the manufacturing of some of the elements required for beam shaping. In many cases lithographic techniques for the production of diffractive optical elements with a proper surface structure offer an adequate manufacturing method.

For these most common techniques for the shaping of stationary beams the relevant design procedures are introduced in the following. The effects of coherence of the beam will be discussed briefly. Examples of techniques for the realization of phase elements are sketched. Detailed discussions are deferred to the literature [97Aag, 99Sin, 00Dic].

7.3.2 Beam-shaping techniques and design procedures

The beam-shaping techniques will be described here using the wave-optical scalar paraxial approximation [85Goo1, 86Sie, 87Bor, 05Hod].

The input beam at $z = 0$ in Fig. 7.3.1 can be described properly either by its complex field strength $E_0(\boldsymbol{x}_0) = \sqrt{I_0(\boldsymbol{x}_0)} \cdot \exp\{\mathrm{i}\,\varphi_0(\boldsymbol{x}_0)\}$ for coherent beams or by its mutual intensity $J_0(\boldsymbol{x}_{01};\boldsymbol{x}_{02}) = \langle E_0(\boldsymbol{x}_{01}) \cdot E_0^*(\boldsymbol{x}_{02})\rangle$ for partially coherent beams [85Goo2, 87Bor]. The phase element in Fig. 7.3.1 is described in the complex amplitude transmission approximation [85Goo1, 86Sie, 87Bor, 97Aag, 05Hod]. Thus the field strength of the incoming beam is multiplied by

$$T = \exp\{-\mathrm{i}\,k \cdot d(\boldsymbol{x})\} \tag{7.3.1}$$

with $k = 2\pi/\lambda$. The complex amplitude transmission approximation is admissible if the minimum feature size of d is approximately 10λ.

The optical structure function $d(\boldsymbol{x})$ characterizes the surface structure of the phase element. If the phase element is realized by a mirror the surface profile is given by $Z = -2d$, and for a transmissive element by $Z = d/(n-1)$.

The optical system that transfers the beam from z' to the output plane at z_1 in Fig. 7.3.1 is assumed to be rotationally symmetric. It may be described by a 2×2 ABCD-matrix

$$\mathsf{M} = \begin{pmatrix} A & B \\ C & D \end{pmatrix}, \quad \det(\mathsf{M}) = AD - BC = 1 \tag{7.3.2}$$

transforming geometrical-optical rays according to

$$\begin{pmatrix} \boldsymbol{x}_1 \\ \boldsymbol{u}_1 \end{pmatrix} = \begin{pmatrix} A & B \\ C & D \end{pmatrix} \cdot \begin{pmatrix} \boldsymbol{x}' \\ \boldsymbol{u}' \end{pmatrix}, \quad \text{or written formally} \quad \boldsymbol{\chi}_1 = \mathsf{M} \cdot \boldsymbol{\chi}', \tag{7.3.3}$$

with

$$\boldsymbol{x} = \begin{pmatrix} x \\ y \end{pmatrix}, \quad \boldsymbol{u} = \begin{pmatrix} u_x \\ u_y \end{pmatrix}. \tag{7.3.4}$$

The shorthand notation $\boldsymbol{\chi}$ for the complete set of ray coordinates was introduced for later reference.

In (7.3.3), (7.3.4) (u_x, u_y) are the ray slopes in the corresponding directions. Obviously, the ABCD-system must not be an imaging system ($B = 0$) but should be as far as possible from imaging. Often the optical system is free propagation over a distance or a Fourier-transformation arrangement.

Without loss of generality the phase φ_0 of the incoming beam may be set to zero for further considerations. A non-vanishing φ_0 can be taken into account by a redefinition of d in (7.3.1). Furthermore, splitting the optical transformation in a phase transformation and a subsequent ABCD-transformation allows shifting quadratic terms between the two systems appropriately. This freedom can be used to adapt the range of d to an amount which is suitable for the manufacturing of the phase element.

In the following design principles are outlined which allow to determine the structure function d. Following the typical arrangement of Fig. 7.3.1 the connection between input and output beam must be derived from a transfer analysis as the first step of the design problem. From this connection an equation for the structure function d has to be set up and a solution has to be found.

7.3.2.1 Beam transformation

7.3.2.1.1 Coherent beams

For coherent beams the transfer analysis is performed in terms of the field strengths.

The input field strength $E_0(\boldsymbol{x}_0) = \sqrt{I_0(\boldsymbol{x}_0)}$ is transformed to the field strength $E'(\boldsymbol{x}')$ at the intermediate position $z = z'$ by multiplication with the phase T of (7.3.1):

$$E'(\boldsymbol{x}') = \exp\{-\mathrm{i}\, k \cdot d(\boldsymbol{x}')\} \cdot E_0(\boldsymbol{x}') \; . \tag{7.3.5}$$

The subsequent transfer of E' to $E_1 = \rho_1 \exp\{\mathrm{i}\,\varphi_1\}$ at $z = z_1$ is performed via the Collins integral [86Sie, 05Hod]. There the ABCD-matrix enters:

$$\begin{aligned} E_1(\boldsymbol{x}_1) &= \int \mathrm{d}^2\boldsymbol{x}' \; K_{\mathsf{ABCD}}(\boldsymbol{x}_1; \boldsymbol{x}') \cdot E'(\boldsymbol{x}') \; , \\ K_{\mathsf{ABCD}}(\boldsymbol{x}, \boldsymbol{x}') &= \frac{-\mathrm{i}\, k}{2\,\pi\, B} \exp\left\{\mathrm{i}\,\frac{k}{2B}\,\left(A\boldsymbol{x}'^{\,2} - 2\boldsymbol{x}\cdot\boldsymbol{x}' + D\boldsymbol{x}^2\right)\right\} \; . \end{aligned} \tag{7.3.6}$$

Finally, the complete transfer reads

$$\begin{aligned} E_1(\boldsymbol{x}_1) &= \int \mathrm{d}^2\boldsymbol{x}_0 \; K_{\mathsf{ABCD}}(\boldsymbol{x}_1, \boldsymbol{x}_0) \cdot \exp\{-\mathrm{i}\, k \cdot d(\boldsymbol{x}_0)\} \cdot \sqrt{I_0(\boldsymbol{x}_0)} \\ &= \sqrt{I_1(\boldsymbol{x}_1)} \cdot \exp\{\mathrm{i}\,\varphi_1(\boldsymbol{x}_1)\} \; . \end{aligned} \tag{7.3.7}$$

The task in the design process is to solve this equation for the structure function d under the constraints that I_0 and I_1 are given. Note that the phase φ_1 of the output field is completely unspecified. This phase freedom must be used appropriately to allow for a solution for d [97Aag]. Mathematically it is not known if a strict solution exists at all. However, approximate solutions may be found via the Gerchberg–Saxton iteration procedure [72Ger, 96Hen, 97Aag] specified in Fig. 7.3.2. As the diagram is symmetric either the left upper or the right lower position may be chosen to start the iteration. Plausible guesses or approximations for d may be inserted as start functions for the iteration.

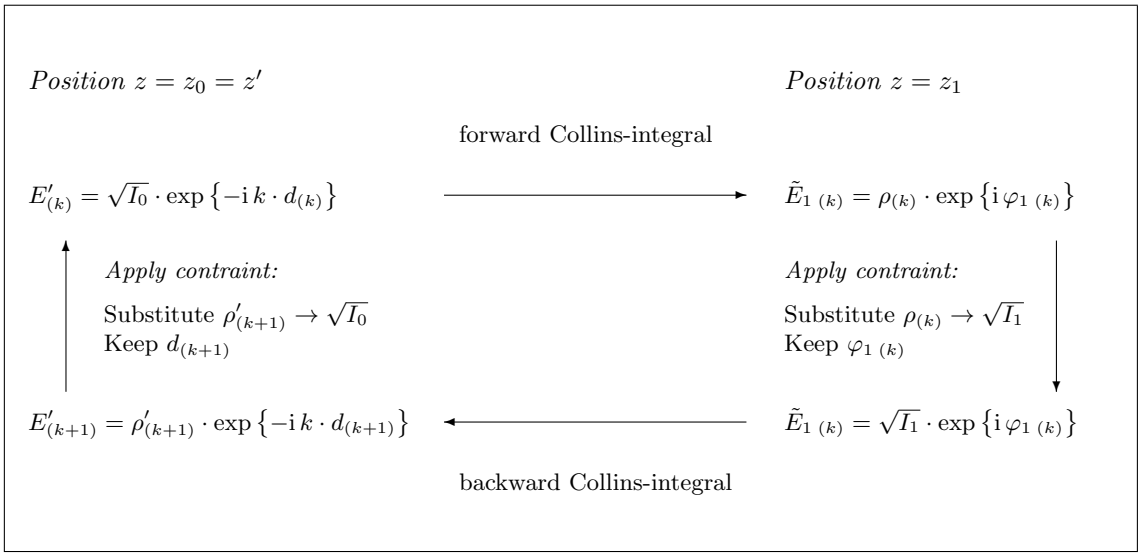

Fig. 7.3.2. Gerchberg–Saxton iteration procedure to solve (7.3.7) for d.

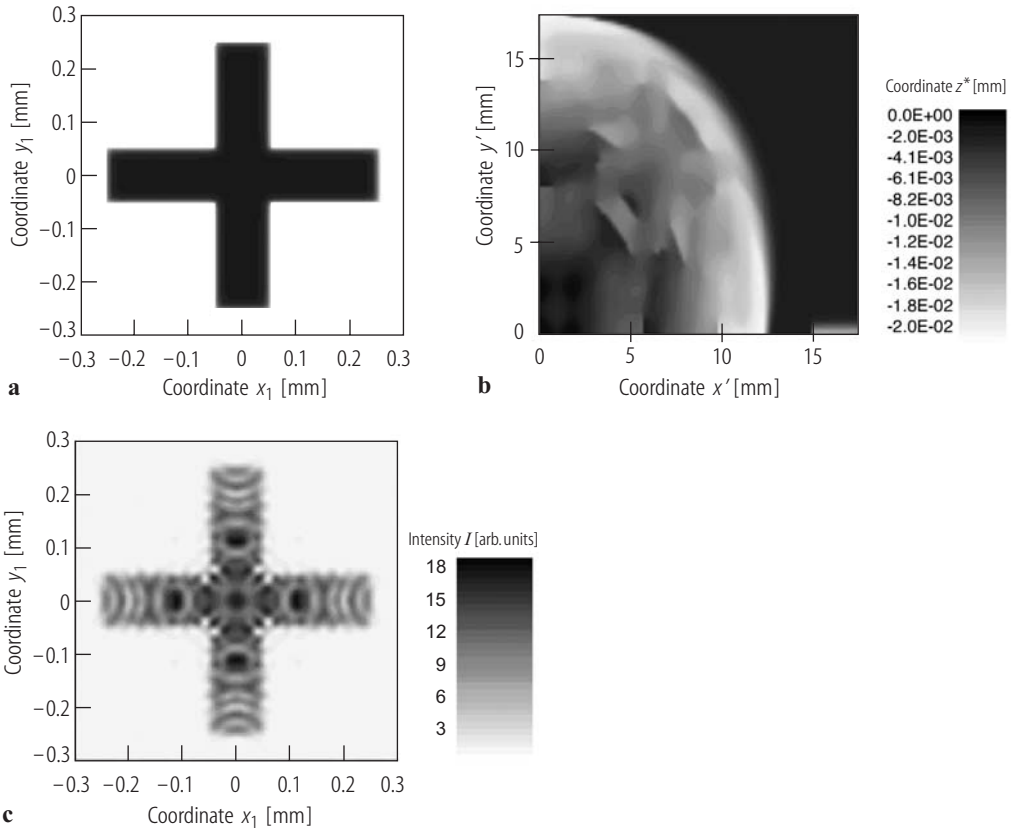

Fig. 7.3.3. Solution of the design problem for the shaping of a homogenously illuminated cross (**a**) from a Gaussian input beam at $\lambda = 10.6$ µm. The iteration result for the surface structure $z^* = -2d$ of a mirror shaping the beam and deflecting it by 45° is shown in (**b**). (**c**) displays the simulation of the beam-shaping process [03Ber].

The quality of the approximation must be observed during the iteration. It can be specified by the transformation efficiency η:

$$\eta_1 = \frac{\int \mathrm{d}^2\boldsymbol{x}_1\, \rho_{(k)}(\boldsymbol{x}_1) \cdot \sqrt{I_1(\boldsymbol{x}_1)}}{\sqrt{\int \mathrm{d}^2\boldsymbol{x}_1\, \left(\rho_{(k)}(\boldsymbol{x}_1)\right)^2 \cdot \int \mathrm{d}^2\boldsymbol{x}_1\, \left(I_1(\boldsymbol{x}_1)\right)}} \tag{7.3.8}$$

which measures the similarity of the shaped PDD with the required I_1.[2] The transformation efficiency is used as a stopping criterion for the iteration in Fig. 7.3.2. An approximate solution for d is found if the iteration does no longer produce significant changes in η_1.

Note that in beam transformation arbitrary phases in the output distribution can be arranged by a second phase element compensating the final phase φ_1, as mentioned in the introduction.

An example for the solution of the design problem of beam transformation is shown in Fig. 7.3.3. Note that in the simulation of the beam-shaping result fluctuations like speckles appear. These may be due to vortex points with a helical structure of the phase comparable to a donut mode. With the help of a demodulation procedure these effects can be reduced to a minimum [03Ber]. If it is necessary to suppress the fluctuations even further contributions from higher spatial frequencies can be directed outside the area of interest within which the output PDD is specified. This amplitude freedom [97Aag] of the output PDD can result in power loss, however.

[2] Alternatively, an analogous expression η' can be computed at position z' from ρ' and $\int I_0$ due to the symmetry of Fig. 7.3.2.

7.3.2.1.2 Partially coherent beams and geometric optic approximation

For the discussion of beam transformation in geometric-optical approximation it is useful to consider partially coherent beams. The discussion can be performed most conveniently not directly with the mutual intensity $J(\boldsymbol{x}_1;\boldsymbol{x}_2) = \langle E(\boldsymbol{x}_1)\cdot E^*(\boldsymbol{x}_2)\rangle$ introduced above but in terms of the Wigner Distribution Function (WDF) $f(\boldsymbol{x};\boldsymbol{u})$ [79Bas, 92Web]. The WDF is derived from J by

$$f(\boldsymbol{x};\boldsymbol{u}) = \frac{k^2}{(2\pi)^2}\int \mathrm{d}^2\boldsymbol{s}\ \exp\{-\mathrm{i}\,k\,\boldsymbol{s}\cdot\boldsymbol{u}\}\cdot\left\langle E\left(\boldsymbol{x}+\frac{\boldsymbol{s}}{2}\right)\cdot E^*\left(\boldsymbol{x}-\frac{\boldsymbol{s}}{2}\right)\right\rangle\ , \tag{7.3.9a}$$

$$\boldsymbol{x} = \frac{\boldsymbol{x}_1+\boldsymbol{x}_2}{2}\ ,\quad \boldsymbol{s} = \boldsymbol{x}_2-\boldsymbol{x}_1 \tag{7.3.9b}$$

with the vector notation of (7.3.4). By (7.3.9b) the coordinates $\boldsymbol{x}$ and $\boldsymbol{s}$ in (7.3.9a) are sum and difference of the two coordinates $\boldsymbol{x_1}$, $\boldsymbol{x_2}$ at which the field strengths E in (7.3.9a) are taken. The arguments $\boldsymbol{x}$, $\boldsymbol{u}$ of the WDF may be interpreted as ray coordinates, see (7.3.4). In the geometric-optical limit the expression $f(\boldsymbol{x};\boldsymbol{u})\ \mathrm{d}^2\boldsymbol{x}\ \mathrm{d}^2\boldsymbol{u} = \mathrm{d}P$ gives the power fraction $\mathrm{d}P$ which is transported from the area element $\mathrm{d}^2\boldsymbol{x}$ at the point (x,y) into the space-angle element $\mathrm{d}^2\boldsymbol{u}$ in the direction (u_x,u_y) by the corresponding rays. In the geometric-optical approach f is the paraxial approximation of the radiance function of photometry.

The intensity I is found from the WDF (7.3.9a) as

$$I(\boldsymbol{x}) = \int \mathrm{d}^2\,\boldsymbol{u}\ f(\boldsymbol{x};\boldsymbol{u})\ . \tag{7.3.10}$$

Following Fig. 7.3.1 the beam-transfer analysis starts from an input WDF f_0. Transit through the phase element is described by a convolution of f_0 with a transmission function τ. Explicitly this reads

$$f'(\boldsymbol{x}',\boldsymbol{u}') = f_0(\boldsymbol{x}',\boldsymbol{u}')\ \otimes_u\ \tau(\boldsymbol{x}',\boldsymbol{u}')\ , \tag{7.3.11}$$

$$\tau(\boldsymbol{x},\boldsymbol{u}) = \frac{k^2}{(2\pi)^2}\int \mathrm{d}^2\,\boldsymbol{s}\ \exp\{-\mathrm{i}\,k\,\boldsymbol{s}\cdot\boldsymbol{u}\}\ T\left(\boldsymbol{x}+\frac{\boldsymbol{s}}{2}\right)\cdot\ T^*\left(\boldsymbol{x}-\frac{\boldsymbol{s}}{2}\right)\ , \tag{7.3.12}$$

where the subscript u in (7.3.11) indicates that convolution is performed with respect to the variable u only.

The form (7.3.1) has to be used in the product $T\cdot T^*$ in (7.3.12). For sufficiently smooth structure functions d an expansion with respect to the variable $\boldsymbol{s}$ can be performed and only the lowest non-vanishing order needs to be kept. In this approximation the transmission function τ reads

$$\tau(\boldsymbol{x},\boldsymbol{u}) = \delta\left(\boldsymbol{u}+\nabla d(\boldsymbol{x})\right) \tag{7.3.13}$$

with δ the Dirac delta function. Thus the convolution in (7.3.11) now merely acts as redefinition of the ray slope $\boldsymbol{u}$:

$$\boldsymbol{u}_0 \to \boldsymbol{u}' = \boldsymbol{u}_0 - \nabla d(\boldsymbol{x}_0)\ . \tag{7.3.14}$$

This transformation property could have been expected in the geometric-optical approximation.

Transfer through the subsequent ABCD-system in Fig. 7.3.1 can be described without approximation using the ABCD-transformation properties of the WDF $f_1(\boldsymbol{\chi}_1) = f'(\boldsymbol{\chi}')$ or $f_1(\boldsymbol{\chi}_1) = f'(\mathsf{M}^{-1}\boldsymbol{\chi}_1)$ and the transformation of the ray coordinates (7.3.3) [79Bas, 92Web, 05Hod]. Consequently, in this approach the transfer through the optical system of Fig. 7.3.1 is described completely in geometric-optical terms.

Combining the transformations and using (7.3.10) an integral expression for the output PDD in terms of the input WDF and the structure function d is obtained. The remaining integral can be done in a saddle-point or rotating-phase approximation [87Bor, 96Hen]. Together with the

assumption of a vanishing phase φ_0 of the input beam this amounts to the use of $f_0(\boldsymbol{x};\boldsymbol{u}) = I_0(\boldsymbol{x}) \cdot \delta(\boldsymbol{u})$ as input WDF. This shows that the divergence angle of the incoming beam must be smaller than the typical deflection angles $|\nabla d|$.

The transfer analysis finally yields the following equation for the structure function d

$$I_0(\boldsymbol{x}_0) = \det\left(\frac{\partial \boldsymbol{x}_1}{\partial \boldsymbol{x}_0}\right) \cdot I_1(\boldsymbol{x}_1) \;, \quad \boldsymbol{x}_1 = A\,\boldsymbol{x}_0 - B\,\nabla d(\boldsymbol{x}_0) \tag{7.3.15a}$$

or explicitely

$$\begin{aligned} \frac{I_0(\boldsymbol{x})}{I_1(A\boldsymbol{x} - B\,\nabla d(\boldsymbol{x}))} &= \det(A\,\delta_{ij} - B\;\partial_i\partial_j d(\boldsymbol{x})) \\ &= A^2 - AB\cdot(\partial_x^2 + \partial_y^2)\,d + B^2\cdot\left(\partial_x^2 d\;\partial_y^2 d - (\partial_x\partial_y d)^2\right) \;. \end{aligned} \tag{7.3.15b}$$

This is a complicated nonlinear second-order partial differential equation for d. It may be solved by an iteration procedure [03Ber]. The equation may be interpreted in terms of the differential geometry of the surface described by d [03Ber].

The structure of the equations (7.3.15a) already results from the relation $I(\boldsymbol{x}_0)\mathrm{d}^2\boldsymbol{x}_0 = I(\boldsymbol{x}_1)\mathrm{d}^2\boldsymbol{x}_1$ together with the coordinate transformation in (7.3.15a). This asserts that there is a one-to-one mapping $\boldsymbol{x}_1(\boldsymbol{x}_0)$ which is assumed in beam transformation.

For problems which separate in the coordinates x, y, i.e. $I(x,y) = \tilde{I}(x)\cdot\hat{I}(y)$ and $d(x,y) = d_x(x) + d_y(y)$, equation (7.3.15a) splits in sets of separately integrable first-order ordinary differential equations

$$\tilde{I}_0(x_0)\,\mathrm{d}x_0 = \tilde{I}_1(x_1)\,\mathrm{d}x_1 \;, \tag{7.3.16}$$

$$x_1 = x_1(x_0) = A\cdot x_0 - B\cdot\frac{\mathrm{d}}{\mathrm{d}x_0}d_x(x_0) \tag{7.3.17}$$

and a similar set for the variable y. Equation (7.3.16) determines the coordinate mapping $x_1(x_0)$, equation (7.3.17) can be integrated to find the structure function d. The solutions of the equations for x, y solve the design problem in the case of separation. With the help of (7.3.16), (7.3.17) even analytic solutions can be found, e.g. the beam-shaping transformation of a Gaussian to a homogenous rectangular tophat distribution [97Aag].

7.3.2.1.3 Comparison of the geometric-optical solution with the solution from the coherent techniques

Figure 7.3.4 shows for a one-dimensional example the comparison of the geometric-optical solution with the solution from the coherent techniques shown above [96Hen].

As in the example of Fig. 7.3.4 the geometric-optical solution of the design problem often is a satisfactory approximation by itself. Alternatively, start functions for the iteration of Fig. 7.3.2 can be found from the geometric-optical techniques shown here.

7.3.2.2 Beam integration

Beam-integration techniques have been developed to solve the most prominent problem of beam shaping, i.e. to generate a highly homogenous rectangular tophat profile from an arbitrary input beam. The basic idea has been outlined in the introduction. Beam integration can be realized by many different systems like caleidoscopes, beam pipes or integrators. Only multifaceted beam integrators are discussed here as only these systems may be described in the arrangement of Fig. 7.3.1. The basic building element is a lens or a mirror with plane facets on a spherical enveloping

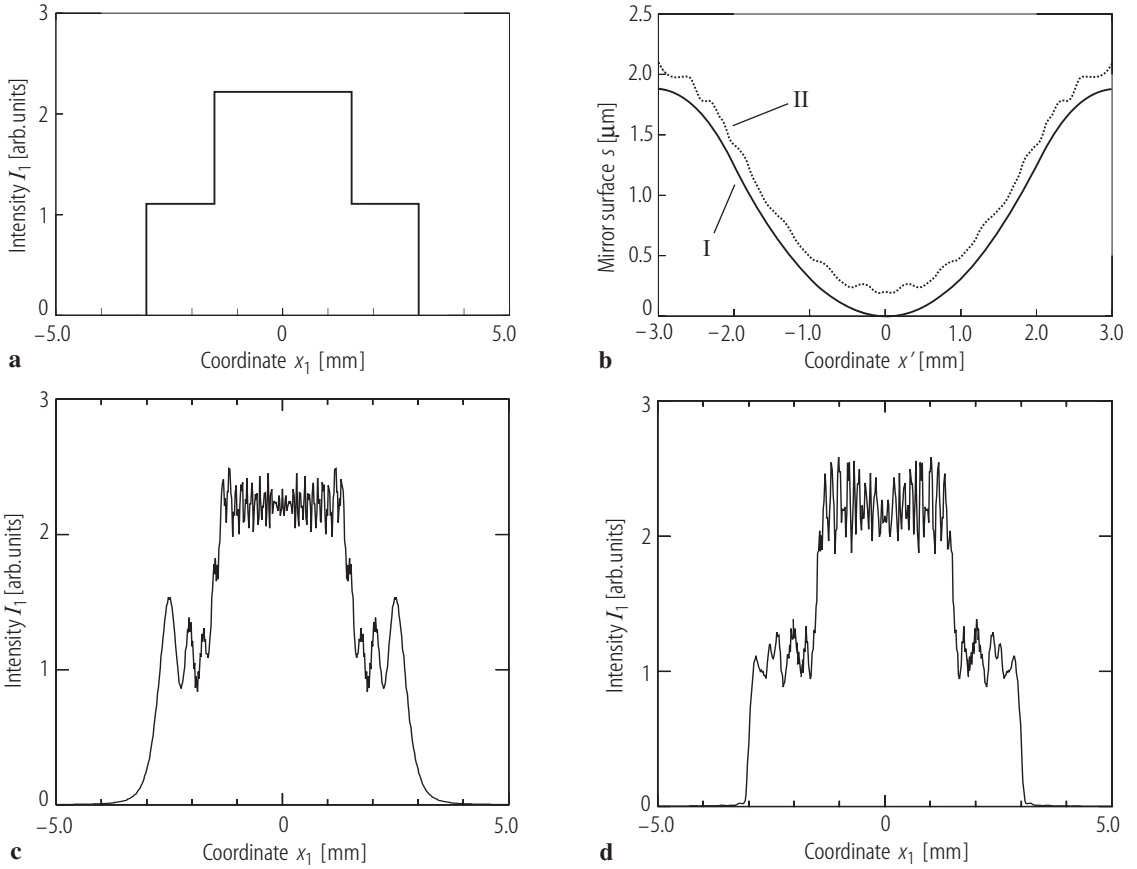

Fig. 7.3.4. One-dimensional example of beam shaping by beam transformation [96Hen]. The desired output PDD (**a**) is formed from a plane-wave input. In (**b**) the mirror surface function obtained by the geometric-optical approach I and by the Gerchberg–Saxton iteration II (curve shifted for convenience) are shown. The beam-shaping simulation for surface I is seen in (**c**), for surface II in (**d**).

surface. For discussion it is simpler to think of these elements as combination of a lenslet array and a focusing lens [96Hen, 98Unn, 99Pah]. Figure 7.3.5 shows examples of integrators composed of these elements.

Imaging integrators as in Fig. 7.3.5a are not strictly in the class described by Fig. 7.3.1. However, due to the imaging principle not only highly homogenous profiles but also very steeply ascending and falling edges can be obtained. Tophat profiles are approximated very well [98Unn].

The arrangement of non-imaging multifaceted beam integrators as in Fig. 7.3.5b strictly follows Fig. 7.3.1. The advantage that only one lenslet array is needed is bought at the expense of reduced edge steepness in the shaped PDD. However, for non-imaging integrators, Fig. 7.3.5b, it is possible to generalize the concept of beam integration to include beam transformation [96Hen] so that this integrator will be discussed.

A discussion of the non-imaging integrator in the framework of the geometric-optical approach of the previous section is of no use as it simply reproduces the basic expectation outlined in the introduction.

The transfer analysis through the system in the framework of the coherent approach is restricted to one transverse beam dimension for simplicity. The discussion will follow the arrangement of Fig. 7.3.5b [96Hen]. All length scales are normalized to the half facet width a, e.g. the transverse coordinate is $\xi = x/a$.

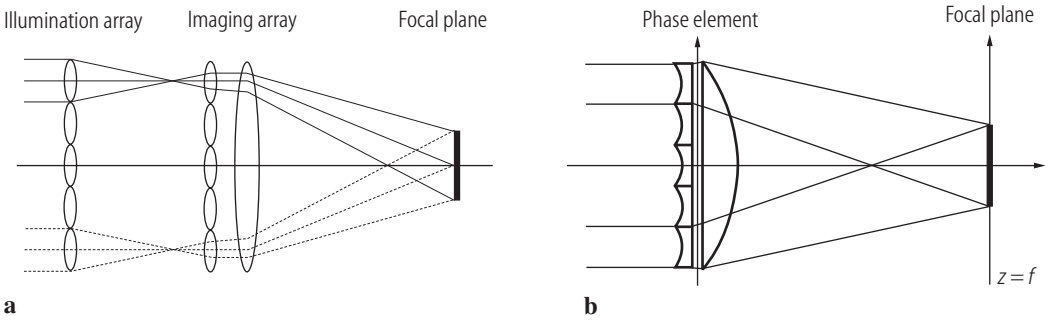

Fig. 7.3.5. Multifaceted beam integrators. (**a**) Imaging integrator or flies-eye integrator. The illumination array is imaged and superposed in the focal plane by the the imaging array. (**b**) Non-imaging integrator.

The transmission function of the lenslet array is the convolution of an array G of δ-functions with the transmission function T_F of the single facet respectively lenslet:

$$T(\xi) = G(\xi) \otimes T_\mathrm{F}(\xi) \,,$$
$$G(\xi) = \sum_{n=-N}^{N} \delta(\xi - 2n) \,, \quad T_\mathrm{F}(\xi) = \mathrm{rect}(\xi) \cdot \exp\{-\mathrm{i}\, k \cdot S_\mathrm{F}(\xi)\} \,. \tag{7.3.18}$$

Here the rect-function describes the boundaries of the facet. The facet or lenslet structure function S_F encodes its interior phase-transmission properties. A standard multifaceted integrator lens needs spheric lenslets $S_\mathrm{F} \propto \xi^2$. The transmission function of the single lenslet T_F becomes

$$T_\mathrm{F}(\xi) = \mathrm{rect}(\xi) \cdot \exp\left\{\mathrm{i}\,\pi\, N_\mathrm{F}\, \xi^2\right\} \tag{7.3.19}$$

with $N_\mathrm{F} = a^2/\lambda f$ the Fresnel number of the arrangement in Fig. 7.3.5b. So the lenslet curvature in (7.3.19) compensates the curvature of the subsequent focusing lens and thus mimics a lens with plane facets. The beam behind the lenslet array may be written as

$$E'(\xi) = E_0(\xi) \cdot (G(\xi) \otimes T_\mathrm{F}(\xi)) \,. \tag{7.3.20}$$

The remaining step in the transfer analysis is the propagation through the focusing lens to the focal plane in Fig. 7.3.5b. Using (7.3.6) this amounts to a Fourier transformation $\mathcal{F}$ and up to an inessential phase factor the output field E_1 reads

$$E_1(\xi) = \mathcal{F}\,[E_0 \cdot (G \otimes T_\mathrm{F})] = \mathcal{F}\,[E_0] \otimes (\mathcal{F}\,[G] \cdot \mathcal{F}\,[T_\mathrm{F}]\,) \,, \tag{7.3.21}$$

where the Fourier transform $\mathcal{F}$ of some function $h(\xi)$ here is defined as

$$\mathcal{F}\,[h(\xi)] = \int \mathrm{d}\,\xi'\, h(\xi') \cdot \exp\{-\mathrm{i}\, 2\,\pi\, N_\mathrm{F}\, \xi \cdot \xi'\} \,.$$

For the Fourier transform of the δ-array one finds

$$\mathcal{F}\,[G] = \sum_{n=-N}^{N} \exp\{-\mathrm{i}\, 4\,\pi\, N_\mathrm{F}\, n \cdot \xi\} \tag{7.3.22}$$

expressing the interference of plane waves from the beamlets. The sum can be evaluated to an array of δ-functions. According to the bracket in (7.3.21) the peak array is modulated by the diffraction pattern of the facet transfer function. Due to the convolution each peak gets the form and width of the Fourier transform of the input field, cf. Fig. 7.3.6. The beam shaping solely shows in the modulation of the peak array.

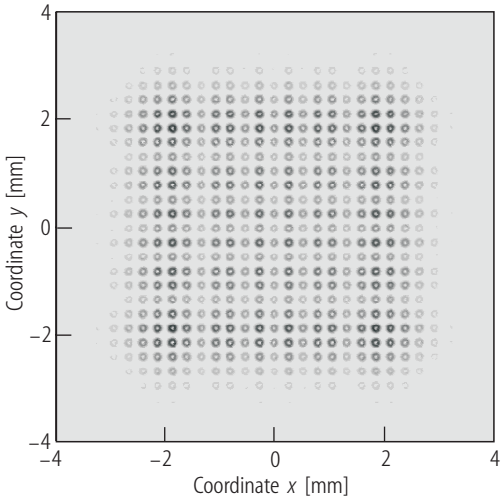

Fig. 7.3.6. Output intensity of a beam integrator with plane facets with the structure according to (7.3.24). The Fresnel number is $N_F = 24$, input beam is a donut mode [96Hen].

A necessary condition [96Hen] for the peak array to exist is that the distance $\Delta\xi$ of the peaks exceeds the peak diameter $2w_f$, i.e. $w_f/(\Delta\xi/2) < 1$, where w_f is the beam radius of $\mathcal{F}[E_0]$. Expressing w_f, $\Delta\xi$ in terms of the parameters of the optical system and the input beam one finds

$$\frac{w_0}{a} \geq \frac{4}{\pi} \cdot M^2 \tag{7.3.23}$$

with w_0 the beam waist radius of the input beam and M^2 the beam propagation factor [92Web, 05Hod]. w_0/a in (7.3.23) roughly estimates the minimum number of facets that have to be illuminated by the input beam for the interference pattern to appear and the beam integration to be successful. This is also necessary for the assumption that within a facet the wavefront may be approximated by a plane wave.

The output power density of the beam integrator in Fig. 7.3.5b reads for coherent illumination [96Hen]

$$I_{coh}(\xi) = \frac{1}{16} N_F^2 \sum_{n=-N}^{N} \tilde{I}_0(\xi - n \cdot \Delta\xi) \cdot \tilde{I}_F(n \cdot \Delta\xi) \tag{7.3.24}$$

with

$$\tilde{I}_0(\xi) = |\mathcal{F}[E_0(\xi)]|^2 \ , \quad \tilde{I}_F(\xi) = |\mathcal{F}[T_F(\xi)]|^2 \ , \quad \Delta\xi = \frac{1}{2N_F} \ . \tag{7.3.25}$$

The first term in the sum in (7.3.24) describes an array of peaks each of the same form as the input beam would obtain when propagated through the system without the lenslet array. The peak distance is given by $\Delta\xi$. This array of peaks is modulated by the intensity pattern of the Fourier transform of the facet transfer function T_F. For plane facets this is the near-field diffraction pattern of a slit or rectangular aperture in two dimensions. Figure 7.3.6 shows an example.

Although the derivation has been done for a coherent laser beam it can be shown that this structure also holds for partially coherent multimode beams [96Hen].

Note that the Fourier transform inverts the length scales of the input in (7.3.24): facets, i.e. the small scales of the input determine the envelope, that is the large scale of the output. The larger scale of the input beam diameter determines the small scale of the peaks. The large scale structure of the output PDD does not depend on the input PDD but only on the facets. As desired beam shaping becomes independent of the input beam.

In many applications with smoothing properties like materials processing the peaked structure of the output is unessential and the beam-shaping result is satisfactory.

For plane-facet integrators the only free parameter which enters the transfer analysis is the Fresnel number $N_F = a^2/\lambda f$. Thus the design problem is reduced to choosing a proper value for N_F and to adjusting a, f correspondingly. The choice of N_F may for example be dictated by the maximum peak distance $\Delta\xi$ (7.3.25) which is allowed by the materials processing application [96Hen].

7.3.2.3 Beam integration with beamlet shaping

The advantage of beam integration is that the beam shaping is independent of the input PDD. The advantage of beam transformation is found in the flexibility of the form of the output PDD. The aim of beam integration with beamlet shaping is to combine these advantages.

In the previous sections it has already been shown in which sense this can be realized. Following (7.3.24) the desired PDD is generated as the function I_F which modulates the peak array of the interfering beamlets. Thus each facet by itself must form a desired output PDD I_1 in the focal plane in Fig. 7.3.5b. The transmission function of the facet now reads

$$T_F(\xi) = \exp\{-i\,k \cdot S_F(\xi)\} = \exp\left\{i\,\pi\,N_F\,\xi^2 - i\,k\,d_F(\xi)\right\} \ . \tag{7.3.26}$$

The non-parabolic contribution d_F in the surface function S_F must be determined so that the second equation in (7.3.25) is satisfied with $I_1 = I_F$. With the techniques of Sect. 7.3.2.1 an appropriate d_F can be found such that the desired PDD I_1 is formed from a plane-wave segment as input beam. In the computations the parameters $A = 0$, $B = f$, $C = -1/f$, $D = 1$ have to be used, cf. Fig. 7.3.5b. The beam transformation in Fig. 7.3.4 is an example for shaping of a single beamlet. Figure 7.3.7 shows the result of beam integration with beamlet shaping with superposed beamlets according to (7.3.24).

For two-dimensional beam shaping often the surface structure function has discontinuities at the facet boundaries. This is unsuitable for manufacturing. Discontinuities can be improved or even avoided, if appropriately curved facet boundaries are admitted [03Ber]. In this case the facets often are grouped in non-orthogonal lattices.

Beam integration with beamlet shaping can produce very satisfactory beam-shaping results even if deviations of the input beam from the specified situation occur. However, the crucial assumption in the design procedure is that the input beam for the beam shaping of each facet is a plane-wave segment. Note that different from the situation in pure beam transformation the phase of the input beam must not be assumed to vanish. It cannot be absorbed in a redefinition of the overall transmission function of the facetted phase element in Fig. 7.3.5b. It may be assumed, however, that the input beam phase is flat on a large scale. Thus there are no quadratic contributions, these could be absorbed in a redefinition of the focusing lens. The deviations caused by local phase front

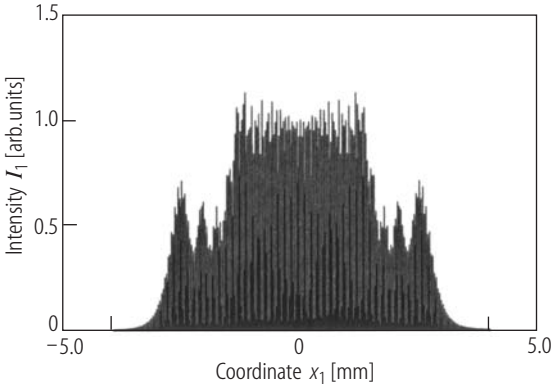

Fig. 7.3.7. Computed output PDD for one-dimensional line integration with beamlet shaping as shown in Fig. 7.3.4. The dense interference structure at wavelength $\lambda = 1.06$ µm makes the PDD quasicontinuous.

deformations can be modeled by the assumption that the input plane waves incident on the facets vary slightly in the incidence angle. Due to the Fourier transform in (7.3.21), (7.3.24), (7.3.25) this shows as slight displacements of the PDDs from the various facets in the output PDD. Thus the desired profile and edges are flattened. The size of facets and the input beam have to be adapted properly to avoid this. As phase deformations may occur as result of partial coherence, too, the subject is discussed further in this framework.

7.3.2.4 Beam shaping and coherence

Like the stationary phase deformations discussed in the previous section statistical fluctuations degrade the quality of beam shaping, too. The induced partial coherence of the input beam may even spoil beam shaping.

As pointed out at the beginning of Sect. 7.3.2 a partially coherent laser beam may be described by its mutual intensity J. Often the mutual intensity can be expressed in terms of a quasihomogenous Schell model beam [77Car, 87Bor]:

$$J(\boldsymbol{x}_1;\boldsymbol{x}_2) = I(\boldsymbol{x}) \cdot \mu(\boldsymbol{s}) \tag{7.3.27}$$

with $\boldsymbol{x}$ and $\boldsymbol{s}$ as defined in (7.3.9b). Here μ is the degree of coherence. The degree of coherence in many cases is described well by a Gaussian function with a width parameter σ which is the transverse coherence length. The model applies well not only for fiber-guided Nd:YAG laser beams [96Hen] or for excimer laser beams [98Unn, 03Ber] but is valid also for the description of beams with statistical phase fluctuations [96Hen]. If a quasihomogenous model beam is used as input beam for beam integration the resulting output intensity reads

$$I_{\mathrm{pc}}(\xi) = I_{\mathrm{coh}}(\xi) \otimes \mathcal{F}\left[\mu(\xi)\right] \tag{7.3.28}$$

with I_{coh} from (7.3.24). Remember that all lengths are normalized to half the facet width. Due to the convolution with the Fourier transform $\mathcal{F}[\mu]$ of the degree of coherence the peak array in the coherent intensity pattern is washed out. A criterion for this is in analogy to the derivation of (7.3.24) that the normalized width 2ε of $\mathcal{F}[\mu]$ should exceed the peak distance in the array, i.e.

$$\rho = \frac{\varepsilon}{\Delta\,\xi/2} > 1\ . \tag{7.3.29}$$

ρ is a smoothing parameter for the interference pattern. Expressing ε and $\Delta\,\xi$ in terms of the parameters of the optical system and the input beam the design rule that the ratio σ/a of coherence length and facet width should be of order unity is obtained.

Equation (7.3.29) only sets a lower limit on ρ. Partial coherence, however, not only washes out the peak array in the output PDD but also flattens edges and details of the coherent PDD. This is undesirable. An optimum design has to be found by optimizing the beam-shaping quality with respect to the parameter ρ. In the standard situation ε in (7.3.29) is fixed by the input beam, so $\Delta\,\xi$ has to be varied. This can be done by adding additional quadratic phase terms in the transmission function T_{F} (7.3.26) of the facet. A beam-shaping quality R may be defined in analogy to the beam-shaping efficiency (7.3.8). R has to be computed in dependence of ρ and the optimum value has to be identified for system design. Figure 7.3.8 shows the design procedure for the profile of Fig. 7.3.4 and Fig. 7.3.7 [96Hen].

Vice versa it is possible to alter the coherence properties of a beam to optimize beam shaping. This can be done with a phase-diffusing element in the input beam. Again the smoothing parameter ρ is used in the optimization procedure. Details are deferred to the literature [96Hen].

As has been seen partially coherent beams need a very careful design in adapting the system parameters like facet sizes and curvatures to the beam parameters. However, if the design rules are observed advanced beam-shaping applications like shown in Fig. 7.3.9 can be achieved.

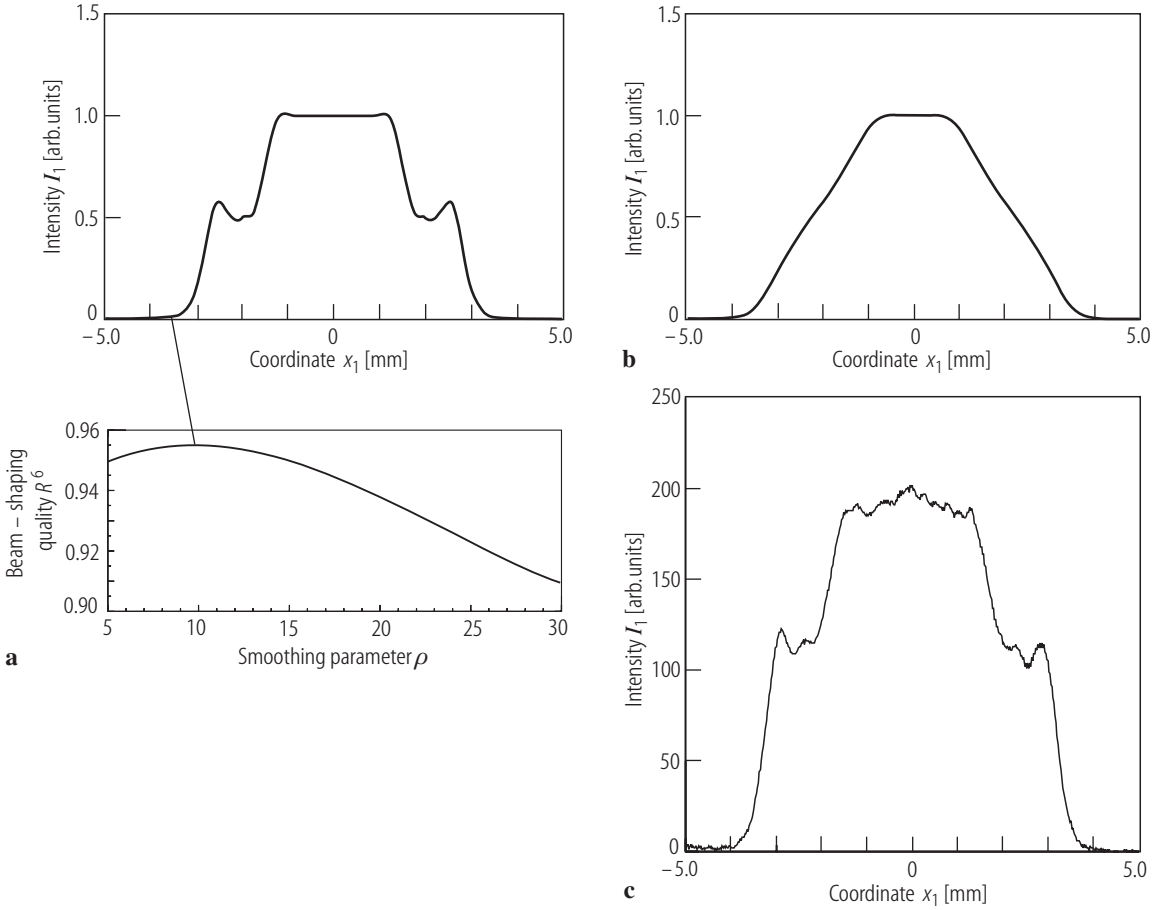

Fig. 7.3.8. (**a**) Optimization of the output beam profile with respect to the smoothing parameter ρ. The intensity diagram corresponds to the maximum of the beam-shaping quality (R^6 for convenience). (**b**) Output beam profile for non-optimized value. (**c**) Measured output PDD of a line integrator manufactured according to optimization in (**a**). $\lambda = 1.06$ μm.

7.3.2.5 Beam splitting

In beam splitting the task is to generate from the input beam an array of beams. Often the output beams in the array are to have approximately equal intensities, but modulated arrays are required in some applications, too. In nearly all cases the input beam is coherent, often a Gaussian.

Usually this problem is thought of in terms of phase gratings with a nontrivial phase function within the slits. Up to different terminology this problem has already been discussed in Sects. 7.3.2.2 and 7.3.2.3. The peak array in the output PDD (7.3.24) exactly solves the task. The freedom of adding additional quadratic phase contributions to the facets can be used to adjust the peak distance in the array. As in Sect. 7.3.2.3 nontrivial phase functions in the facets can be used to adjust the array modulating function.

It must be mentioned that various other techniques for beam splitting or array illumination exist [99Sin]. However, they cannot be arranged as in Fig. 7.3.1 and will not be described here.

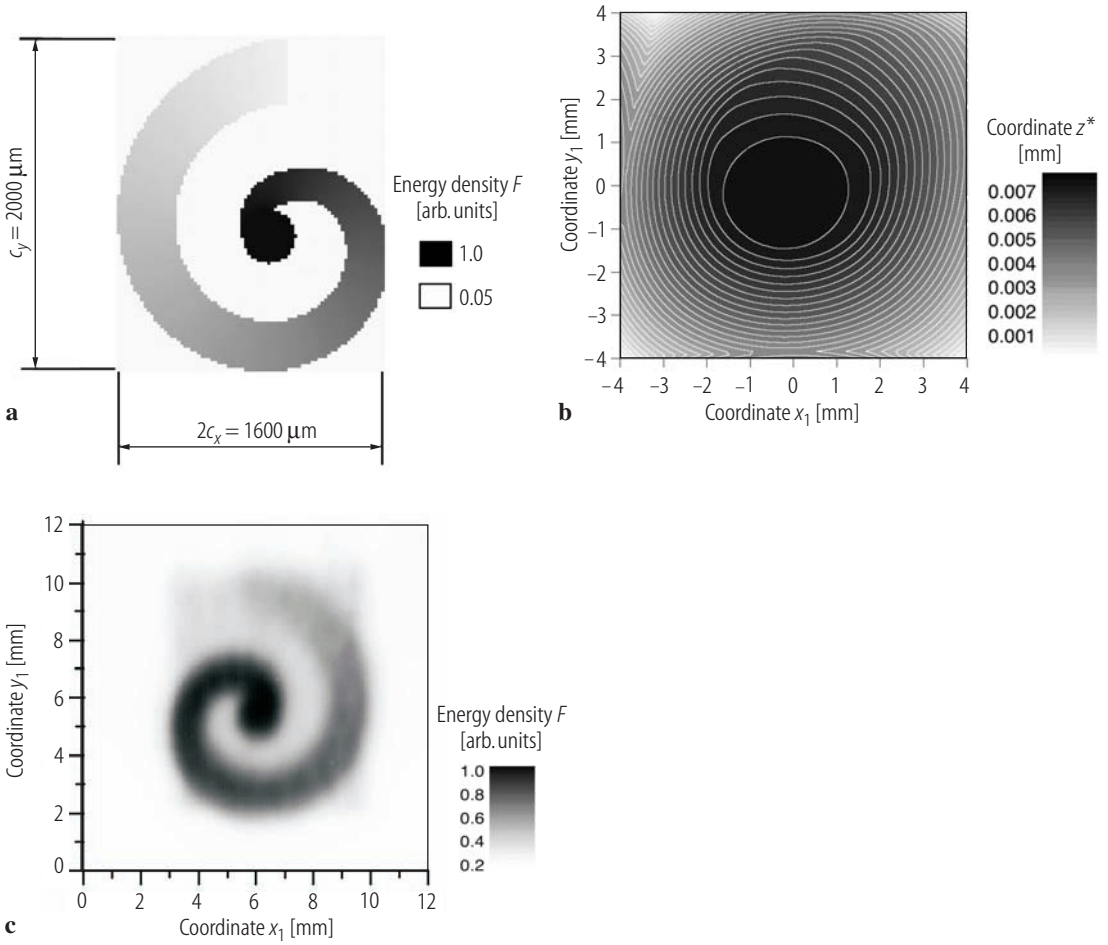

Fig. 7.3.9. Two-dimensional beam integration with beamlet shaping for an eximer laser [03Ber]. (**a**) Desired output PDD, an Archimedic spiral curve. (**b**) Facet surface profile designed with the geometric-optical approach and optimized with respect to the coherence properties of the input beam. (**c**) Measurement of the shaped PDD.

7.3.2.6 Manufacturing of beam-shaping elements

The phase elements of beam-shaping systems can be realized as reflecting, refracting or as diffracting elements with appropriately shaped surfaces. Although GRIN techniques are possible in principle a sufficiently precise adjustment of the local index of refraction is difficult.

Depending on the realization the manufacturing methods are chosen. The main requirement is that the manufacturing techniques have to be able to realize the free form surface given by the structure function $d(x, y)$ in its full range with all its feature sizes with appropriate precision. This is usually $\lambda/10$ of the used wavelength or even better.

For all manufacturing techniques the dynamical range of the surface profile unfortunately must not be too large. Mostly the range is restricted to less than 10. . . 50 µm. It is therefore necessary in the design process to use all degrees of freedom to avoid high dynamical ranges. Most important the freedom to shift quadratic phase contributions to the optical system can be used.

Especially for the manufacturing of diffractive phase elements lithographic techniques can be used with success [99Pah, 99Sin]. For diffractive optical elements the surface profile given by the structure function is realized modulo the wavelength of the beam to be shaped. This corresponds

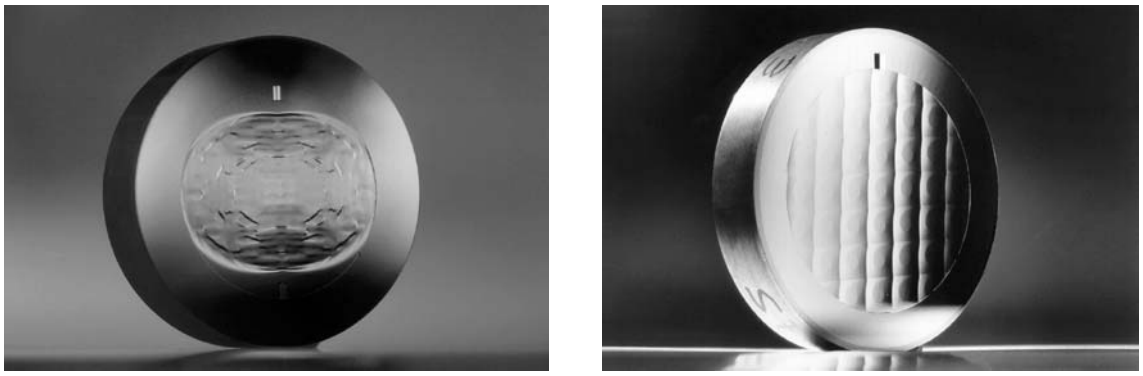

Fig. 7.3.10. Beam-shaping mirrors manufactured by diamond turning [03Ber]. Mirror (**a**) realizes the beam transformation to shape the cross profile discussed in Sect. 7.3.2.1. Mirror (**b**) realizes beam integration with beamlet shaping for the spiral shown in Fig. 7.3.9.

to a restriction of the phase to the range $0 \ldots 2\pi$. Often this leads to feature sizes which are comparable to the wavelength. These are accessible to lithographic techniques. To realize the resulting surface structure both mask lithography and scanning lithography with electron or laser beams is used to expose a photo resist. In subsequent etching steps the surface structure can be generated either as a binary phase element or as blazed phase element. In binary phase elements [96Goe] the phase range $0 \ldots 2\pi$ is divided in a number of levels and the profile given by the structure function is approximated by these levels. For low-level numbers binary phase elements suffer from low efficiency ($\eta = 41\%$ for 2 levels, $\eta = 95\%$ for 8 levels [99Sin]), high-level numbers make manufacturing expensive.

An alternative method is provided by gray-scale lithography [99Sin]. The photo resist is exposed to continuously varying intensity either by electron or laser beam scanning or by the use of gray scale mask. In the subsequent etching the gray scales are transferred as surface profiles.

A very prominent manufacturing technique for reflective and also for refractive phase elements is fast tool servo diamond turning [93Pyr]. In this technique the diamond tip of the turning tool is moved back and forth by piezoelectrical actuators during the revolution of the work piece. According to the manufacturing process the surface profile $Z(r, \varphi)$ is split as

$$Z(r, \varphi) = Z_{\mathrm{rot}}(r) + Z^*(r, \varphi) \tag{7.3.30}$$

in a rotationally symmetric part and a non-rotationally symmetric part. Remember that the surface profile Z and the structure function d are connected by $Z = -d$ for mirrors and $Z = d/(n-1)$ for transmissive elements. The dynamical range of Z^* is restricted as mentioned above.

Furthermore, the mechanics of the process does not allow profiling arbitrary steps in surface. Therefore this technique is mainly suited for smooth surface profiles not realized diffractively. Figure 7.3.10 shows examples of beam-shaping mirrors for applications in materials processing with CO_2 and excimer lasers.

However, the turning process induces a grating structure on the surface which may become disturbing for short wavelengths. Nevertheless for optics manufacturing feature sizes < 5 μm and surface roughness of less than 1 nm has been demonstrated in selected examples.

7.3.3 Conclusion

Design procedures for the most common beam-shaping techniques have been outlined and a brief sketch of the manufacturing of beam-shaping elements has been given. The scalar paraxial approximation has been used throughout the analysis. Especially for the design of diffractive beam-shaping elements and for microoptical elements feature sizes in the order of the wavelength may occur. In the analysis of these elements the full vectorial diffraction theory has to be applied. This goes far beyond the scope of this contribution and may be found in the literature [97Kui]. Furthermore, a lot of other manufacturing techniques have been suggested. The discussion of these techniques is deferred to the literature [99Sin].

References for 7.3

72Ger Gerchberg, R.W., Saxton, W.O.: A practical algorithm for the determination of phase from image and diffraction plane pictures; Optik **35**(2) (1972) 237–246.

77Car Carter, W.H., Wolf, E.: Coherence and radiometry with quasihomogenous planar sources; J. Opt. Soc. Am. **47**(6) (1977) 785–796.

79Bas Bastiaans, M.: Wigner distribution function and its application to first order optics; J. Opt. Soc. Am. **69** (1979) 1710.

85Goo1 Goodman, J.: Introduction to Fourier optics, New York, USA: John Wiley & Sons, 1985.

85Goo2 Goodman, J.: Statistical optics, New York, USA: John Wiley & Sons, 1985.

86Sie Siegman, A.E.: Lasers, Mill Valley, CA: University Science Books, 1986.

87Bor Born, M., Wolf, E.: Principles of Optics, Oxford, UK: Pergamon Press, 1987.

88Dic Dickey, F.M., O'Neil, B.D.: Multifaceted laser beam integrators: general formulation and design concepts; Opt. Eng. **27** (1988) 999.

92Web Weber, H.: Propagation of higher-order intensity moments in quadratic-index media; Opt. Quantum Electron. **24** (1992) 1027.

93Pyr Pyra, M.: Nicht-rotationssymmetrische Laserspiegel – Möglichkeiten und Grenzen der Herstellung, Dissertation, RWTH Aachen, Germany, 1993.

96Goe Goebel, B., Wang, L.L., Tschudi, T.: Multilayer technology for diffractive optical elements; Appl. Opt. **35** (1996) 4490–4493.

96Hen Henning, T.: Strahlformung für die Oberflächenbehandlung mit Hochleistungslasern, Dissertation, RWTH Aachen, Aachen, Germany: Shaker Verlag, 1996.

97Aag Aagedal, H., Wyrowski, F., Schmid, M.: Paraxial beam splitting and shaping, in: Diffractive optics for industrial and commercial applications, Turunen, J., Wyrowski, F. (eds.), Berlin, Germany: Akademie Verlag, 1997, 165–183.

97Kui Kuittinen, M., Turunen, J., Vahimaa, P.: Subwavelength-structured elements, in: Diffractive optics for industrial and commercial applications, Turunen, J., Wyrowski, F. (eds.), Berlin, Germany: Akademie Verlag, 1997, 303–323.

97Leg Leger, J.R.: Laser beam shaping, in: Microoptics: elements, systems and applications, Herzig, H.P. (ed.), London, UK: Taylor & Francis, 1997, 223–257.

98Unn Unnebrink, L.: Strahlformung partiell kohärenter Laserstrahlung: Optimierung eines Beleuchtungssystems für Maskenprojektionsverfahren mit UV-Lasern, Diplomarbeit, RWTH Aachen, Germany, 1998.

99Pah Pahlke, M.: Auslegung hocheffizienter, computergenerierter Beugungsstrukturen zur Strahlformung, Dissertation, Universität Stuttgart, Germany, 1999.

99Sin Sinzinger, S., Jahns, J.: Microoptics, Weinheim, Germany: Wiley-VCH Verlag, 1999.

00Dic Dickey, F.M., Holswade, S.C.: Laser beam shaping: Theory and techniques, New York, USA: Marcel Dekker Inc., 2000.

03Ber Bernges, J.: Auslegung und Anwendung nichtrotationssymmetrischer Optiken für die Laser-Materialbearbeitung, Dissertation, RWTH Aachen, Germany, 2003.

05Hod Hodgson, N., Weber, H.: Optical resonators – fundamentals, advanced concepts, and applications, New York, USA: Springer, 2005.